Research Article | Vol. 26, No. 20 | 1 Oct 2018 | OPTICS EXPRESS 25534
Optics EXPRESS

Single shot, large area metal sintering with micrometer level resolution

NILABH K. ROY,[1] DIPANKAR BEHERA,[1] OBEHI G. DIBUA,[1] CHEE S. FOONG,[2] AND MICHAEL A. CULLINAN[1,*]

[1]*Department of Mechanical Engineering, The University of Texas at Austin, 204 E. Dean Keeton St, Austin, TX- 78712, USA*
[2]*NXP Semiconductors, 6501 W William Cannon Dr, Austin, TX-78735, USA*
**michael.cullinan@austin.utexas.edu*

Abstract- This paper presents the optics design for a microscale Selective Laser Sintering (μ-SLS) system that aims to allow large areas of nanoparticles to be sintered simultaneously while still maintaining micrometer scale feature resolutions in order to improve the throughput of the microscale additive manufacturing process. The optics design is shown to be able to sinter a 2.3 mm by 1.3 mm area of metal nanoparticles that have been spread into a ~400 nm thick layer with a feature resolution of ~3 μm in a single shot. The optical resolution of this system is shown to be ~1.2 μm indicating that only about 2-3 pixels are needed to form a good sintered part. In addition, using the optical design presented in this paper, it is estimated that the μ-SLS system should be able to achieve a volumetric throughput of ~63 mm^3/hr, making this process one of the highest throughput processes available today for the microscale additive manufacturing of three-dimensional metal structures.

1. Introduction

Micro-additive manufacturing (AM) techniques have a multitude of applications in many fields including the aerospace, medical device, automotive and semiconductor industries [1,2]. Focusing on the semiconductor packaging industry, the rate of miniaturization of packaging blocks such as solder bumps, is trailing the miniaturization of transistors due to the limitations of the capabilities of current back end of line fabrication processes [3]. These solder bumps provide interconnects between one die and another or between a die and substrate and, traditionally, they have been manufactured using the electroplating process. With advancements in integration of multiple chips on a single package, the requirements of I/O densities for these chips has far exceeded the density and pitch capabilities provided by the traditional solder bump processes [4,5]. As a result, the industry has adopted pillar bumps to replace these solder bumps as they enable smaller pitches, better electromigration performance and better thermal regulation [6–8]. These pillar bumps are fabricated using the electroplating process with 40-50 μm widths and a maximum height to width aspect ratio of 2 [9]. Producing higher aspect ratio structures is still beyond the capabilities of the current process [10,11]. A promising process for the fabrication of these high aspect ratio pillars with sub-10 μm diameter is to additively manufacture these high density, high aspect ratio interconnect structures.

Many micro-scale AM techniques have been developed with different capabilities to fulfil different functional requirements for e.g. two photon lithography and interference lithography work only with photocurable polymers to produce parts with 100-200 nm feature resolutions [12], other processes such as direct- ink writing and electrohydrodynamic jet printing work with both polymers and metals and can also get the desired sub-μm resolution but are limited to generate only 2D or 2.5D structures [13–15]. A major drawback associated with most of the micro-AM techniques is their scalability to high throughput applications [14–21]. Since the feature resolution in a micro-AM is typically reduced by at least a couple of orders of

#338214 https://doi.org/10.1364/OE.26.025534
Journal © 2018 Received 20 Jul 2018; revised 31 Aug 2018; accepted 31 Aug 2018; published 17 Sep 2018

Optics EXPRESS

magnitude compared to traditional AM processes, the areal throughput can go down by four orders of magnitude or more which makes the implementation of these micro-AM techniques in a high-volume IC packaging setting extremely infeasible and unprofitable. This study presents the optics design for a micro-scale selective laser sintering (μ-SLS) process that enables the sintering of a large area with 1μm feature resolution. The conventional laser sintering process is limited in its resolution to 100 μm due to the use of micro-particles and large laser spot sizes [22,23]. To achieve 1μm feature resolution, use of nanoparticles is required. Recently, laser sintering of nanoparticles has generated much interest as an alternative to conventional IC fabrication techniques and for printed electronics applications [24–26]. Although prior work has been done to achieve fine resolution sintering of metal nanoparticles using short and ultra-short pulsed lasers [27–29], many of the studies have been demonstrated for mono-layer sintering of printed electronics, and typically use a single focused beam for sintering [30,31]. For patterning a complex and large area pattern, the laser beam is raster scanned across the sample. This approach is very slow to be used for production environments such as chip packaging. This study demonstrates the realization of ≈1 μm optical resolution alongwith the capability to sinter a large area at once so that it can be employed in a high-volume production system.

In addition to the optical system design presented in this study, the μ-SLS system includes a spreader system and a sample transfer, alignment & metrology system to produce three dimensional structures with the desired feature resolution. The samples are first coated with nanoparticles using the spreader system and then the coated samples are transferred to the optical system using the sample transfer and alignment system. Once the nanoparticle layer over the wafer is sintered, it is moved back to the spreader for the next layer to be coated and the cycle is repeated until the final part is obtained. The final part goes through a washing step to get rid of the un-sintered portions and then post heat treatment is done to improve the sintering quality of the part. An overview of the system with process details and scheme is part of a working study by the authors [32].

2. Optics design

The primary requirement for the optical sub-system is to be able to reduce the feature resolution to < 5 μm (preferably close to 1 μm). However, focusing the beam to a single spot size of ≈1 μm has a major disadvantage. It reduces the areal throughput of the system by a factor of 10,000 compared to conventional sintering systems with a spot size of 100 μm. To overcome this problem and increase the throughput of the process, a digital micro-mirror device (DMD) is used to replace the galvanometric mirror used in macroscale SLS systems. A DMD is an array of micro-mirrors which can be modulated between two positions- ‘on’ and ‘off’. Depending on the position of the mirrors, the light beam is either reflected along the propagation direction or to the heatsink. The DMD setup uses a DLP chipset- DLP6500 from Texas Instruments containing a 1920 X 1080 array of mirrors (more than 2 million mirrors total) with 7.6 μm micromirror pitch and the mirrors have a 24° illumination cone [33]. The mirrors are 7.0 μm by 7.0 μm in size, placed 600 nm apart, and can be controlled independently with a pattern update rate up to 9500 Hz for a binary pattern. The DLP chipset has a rated damage threshold of 25 W/cm^2 [33]. This DMD can be coupled to a continuous wave (CW) or a pulsed laser (nanosecond or femtosecond) of appropriate power using a fiber coupling and illumination optics setup. For this application, an 808 nm 50 W CW laser (BWT Beijing Ltd.) is employed in the system. With this setup, the throughput of the process is greatly enhanced as instead of sintering just one 1 μm diameter spot, an astounding two million 1 μm square spots are sintered simultaneously. DMDs have been previously used for sintering nanoparticles, however the pattern size per exposure was much smaller than the optics design proposed in this study [24].

The coupling of laser beam to DMD uses a set of optics including a fiber coupler, mirrors and lenses for redirecting and resizing the beam and a fly’s eye lens for reshaping the spatial

Optics EXPRESS

intensity of the beam from a spatially gaussian beam to a top-hat distribution so that all the mirrors in the mirror array get equal intensity of light. This is essential to ensure uniformity in sintering quality across the entire sintered area. This reshaped beam then passes through a set of mirrors and lenses and hits the DMD to fill the entire array. The mirrors then reflect the individual beams into one of the two directions depending upon their position ('on' or 'off'). These beams then pass through the focusing/imaging setup shown in Figs. 1 and 2.

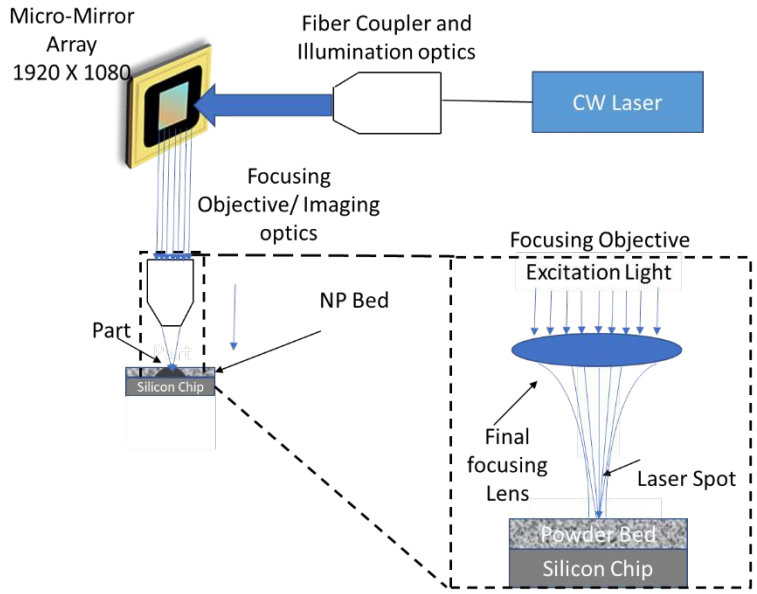

Fig. 1. Schematic showing the optics design for μ-SLS system.

2.1. Imaging optics design

The design requirements for the imaging optics design are: a) To achieve 1 μm resolution and b) To collect maximum possible light reflected off of the DMD to achieve high irradiance for sintering at the sample plane and minimize the exposure duration. Instead of using the off the shelf 1" dia. focusing solutions such as long working distance infinity corrected objectives, a custom focusing/imaging solution is presented below. Focusing solutions available off the shelf generally are designed for 1" optics and do not guarantee maximum light collection due to their smaller apertures. This leads to much smaller irradiances at the sample plane and consequently, longer exposure durations, large heat affected zones and lower throughputs. Additionally, the numerical aperture options for the commercially available long working distance objectives are limited and cannot meet the 1 μm resolution requirement while being cost-effective at the same time.

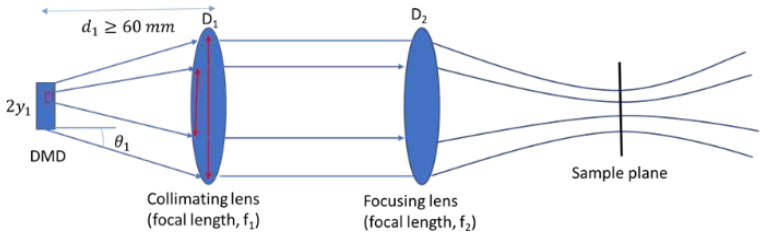

Fig. 2. Cartoon of the proposed imaging optics.

Optics EXPRESS

For maximum light collection, it is ideally required that the aperture of the collimating lens be larger than the beam expanse at the lens location. This constraint can be expressed as:

$$D_1 \geq 2y_1 + 2d_1 \tan(\theta_1) \quad (1)$$

$$\& d_1 \geq 60\,mm\,(DMD\,box\,dimenison\,constraint) \quad (2)$$

where, D_1 is the lens diameter, $2y_1$ is the longer dimension of the DLP chipset, d_1 is the distance between DMD and the collimating lens and $2\theta_1$ is the light cone angle reflected off of the DMD. To maximize the light collection, 50 mm diameter lenses were used. The collimated beam then passes through a focusing lens to image the DMD pattern on the sample plane with the desired resolution. It is critical to verify that the diffraction limited resolution of the focusing lens is smaller than or equal to the desired resolution which in this case is 1 μm. Assuming a top hat laser beam, the following inequality has to be fulfilled to avoid running into diffraction limited resolution issues where, λ is the wavelength of laser used (808 nm), f_2 and D_2 are the focal length and diameter of the focusing lens.

$$d_{diffraction} = \frac{2.44\lambda f_2}{D_2} \approx 1\mu m\,or\,smaller \quad (3)$$

And lastly, given that the size of each mirror is 7 μm and the desired resolution at the image plane is 1 μm, the magnification of the setup which is given as the ratio of the focal lengths of the collimating and focusing lens should follow the following inequality.

$$Magnification, m = \frac{f_2}{f_1} \leq \frac{1\mu m}{7\mu m} \quad (4)$$

Subject to the constraints 1-4, a plano convex lens with a 50 mm diameter and a focal length of 200 mm is selected as the collimating lens. For focusing lens, an aspheric lens with a 50 mm diameter and 30 mm focal length is selected to achieve the desired resolution. This combination has a theoretical magnification of 30/200 = 1/6.66 and considering the diffraction limited resolution of 1.18 μm, each mirror is focused to ~1.2 μm image at the focal plane of the focusing lens. Using an aspheric lens helps with mitigating spherical aberration effects in the system. This optical design achieves the following objectives: (1) Collect maximum possible light reflected out of the DMD box, (2) Achieve ~1 μm resolution, and (3) Produce large area patterning (>2 mm^2)

3. Sample preparation and optical setup

The samples are prepared by spin coating Ag nanoparticle ink (JS-A-102A, Novacentrix, Austin, TX) onto a glass substrate to achieve sub-micron thick layers of Ag nanoparticles. The average particle size of nanoparticles in the ink is between 30 and 50 nm and the primary solvent in the ink is di-ethylene glycol. Figure 3 shows the setup used for sintering Ag nanoparticles using the DMD for patterning large areas. The setup is based on the optical sub-system design presented above. A beam profiler (SP 928, 3.69 μm pixel size, 1928 X 1448 pixels, Ophir electronics) is used for imaging the sample and for focusing the laser beam accurately to achieve the sharpest image resolution. An 808 nm 50 W CW laser is used as the laser source for sintering these nanoparticles. Due to inefficiencies of the illumination setup (losses in the optical elements- lenses, mirrors, fly's eye lens, alignment losses in the illumination setup inside the DMD box), the power loss from fiber-coupling to the DMD is about 55-60%. Thus, with a 50 W input laser power, the power reaching the DMD is around 20 W-22.5 W. The DMD area is about 1.2 cm^2, thus the fluence reaching the DMD is roughly 16.7-18.7 W/cm^2 which is lower than the damage threshold of the DMD used.

Optics EXPRESS

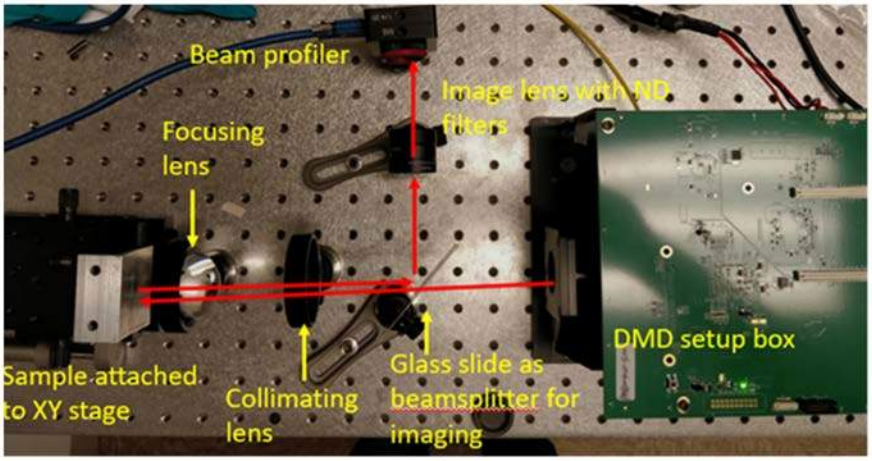

Fig. 3. Experimental setup for sintering with DMD using the optical design presented.

The patterns are created either programmatically or by format conversion of logos/images to monochrome bitmap images and then are uploaded to the DMD using the DLP 6500 GUI. The pattern image is sized to match the pixel ratio and pixel count on the DMD. Once the pattern has been uploaded to the DMD, the laser is turned on for the desired exposure duration and the sample is sintered. The exposure duration for sintering is controlled through the DLP 6500 GUI. The sintered sample is then placed in a container with iso-propyl alcohol and the sample is agitated using a tip-ultrasonicator (Qsonica, Q500, 1/2" tip with a maximum amplitude of 120 μm) for 45 s with an oscillation amplitude of 24 μm to wash off the un-sintered portion of the sample. The un-sintered portion of the sample is easily dissolved in the solvent while the sintered portion sticks to the glass substrate showing good adhesion strength between the sintered portion and glass. This allows for recovery of the un-sintered inks by using the primary solvent of the ink for ultrasonication and then post-treatment of the collected suspension to achieve parent ink characteristics. It reduces the overall material costs significantly for the process. The samples are then imaged under either an optical microscope or a scanning electron microscope (FEI Quanta 650) for further analysis. Surface topography images of the sample are obtained using an optical profilometer (Wyko NT 9100 Optical profilometer).

4. Resolution

The magnification of the setup can be calculated as the ratio of the size of the image on the DMD chip to the size of image obtained at the sample plane (see Fig. 4). The length of DMD chip is approximately 14.59 mm (= 1920* 7.6 μm). An array of vertical lines and a Texas Longhorn patterns are projected onto the DMD as shown in Fig. 4. The pattern length and width are 1920 X 1080 pixels and are expected to completely fill the DMD chip. Black pixels require the corresponding mirror to be 'off' and white pixels are 'on'. The image at the sample plane is collected by placing the beam profiler at the sample plane location and the ratio of the two image sizes (at the DMD chip and sample plane) is computed to get the magnification.

$$Demagnification\,along\,the\,length = \frac{Length\,of\,the\,DMD\,chip}{Length\,of\,the\,image} = \frac{14.59}{2.34} = 6.23 \quad (5)$$

$$Demagnification\,along\,the\,width = \frac{Width\,of\,the\,DMD\,chip}{Width\,of\,the\,image} = \frac{8.21}{1.23} = 6.22 \quad (6)$$

Optics EXPRESS

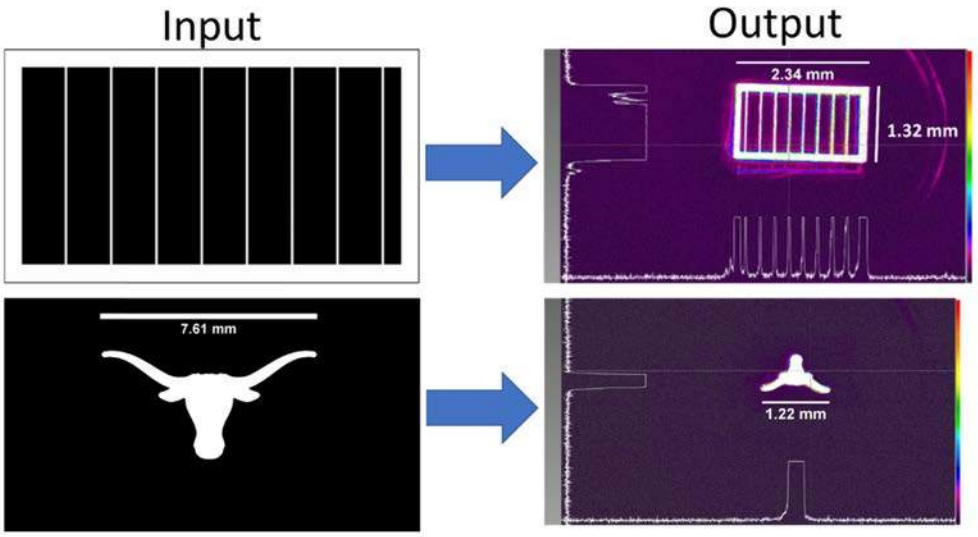

Fig. 4. Figure showing reduction in pattern sizes at the sample plane when compared to the input image at the DMD plane (a) pattern is an array of vertical lines with 10 μm line width, 200 μm spacing and 80 μm boundary (b) a Texas Longhorn logo with an end to end size of 7.61 mm.

Using the above two sets of patterns, the demagnifications are calculated to be 6.23 and 6.22 along the length and width of the image respectively. This is very close to the expected de-magnification of 6.66 as calculated earlier based on the focal lengths of the collimating and focusing lens used. The estimated resolution using a de-magnification of 6.23 is found to be 1.12 μm (= 7/6.23) which is close to the desired resolution of 1 μm and diffraction limited resolution of 1.18 μm. Thus, the optical design is able to achieve the desired resolution of ~1 μm.

5. Sintering results

Figure 5 shows different sintered patterns demonstrating the large area, fine resolution sintering capability of the system. Sintering exposure durations for the sintered patterns shown below are between 5 s and 10 s. Part a) of the Fig. 5 shows a high magnification SEM image of an unwashed sample with 10 μm line thickness. As can be seen from the SEM image, the particles within the line appear to be sintered well when compared to the surrounding region. Part b) of the Fig. shows a thinner sintered line- 3 μm wide and demonstrates the sintering resolution achievable with the current hardware. It appears that 2-3 pixels are required to create good sintering in the bed using the current setup. One of the primary reasons for difficulty in achieving the 1.2 μm feature resolution with the current setup is that the exposure durations are very long and as a result, heat affected zones (HAZs) are significant. The effect of HAZ on feature resolution can be alleviated by using a higher power laser at the source so that the sintering irradiances are higher and the sintering temperature in the particle bed can be reached in shorter duration. This means shorter exposures and as a result, smaller conduction induced HAZs in the particle bed. Another contributing factor to the larger feature resolution (compared to the estimate presented above) and non-uniformity in sintering across large area patterns could be the imperfect focusing of the sample. Since the Rayleigh range for these feature sizes are on the same order as the least count of micrometer screw of XY stage, achieving perfect focusing of the sample across the entire spot area is extremely difficult. Thus, there is a need for more precise positioning and alignment of the stage with respect to the incoming laser beam to achieve better resolution. The pattern in part c) is a Texas Longhorn with an end-to-end dimension of 0.88 mm and shows both the large

Optics EXPRESS

area and complex pattern capability of the system. Parts d), e) and f) show portions of different large area periodic patterns (2.3 mm by 1.3 mm) which comprise of circular spots with different diameters and pitches. Parts d) and e) show periodic patterns with 40 μm diameter circles with 80 μm pitch and part f) shows a pattern with 10 μm diameter circles with 40 μm pitch. These images show the feasibility of producing pillar structures for IC packaging with much smaller diameters and pitches than the current capabilities of the electroplating process. These structures can be produced by additively building up these pillars using the layer-by-layer approach. To assess the sintering quality of the sintered structures, the electrical resistivity of sintered lines is found to be 57.25 x 10^{-8} Ω-m. The sintered samples are heated on a hot plate at 150°C for 30 min for further reducing the resistivity of the samples. Resistivity of post processed samples is found to be 7.28 x10^{-8} Ω-m which is 4.5 times the bulk resistivity of Ag and similar to or better than conductivity of sintered Ag reported in literature [24,34,35]. The thickness of the un-sintered ink for most samples is between 350 and 400 nm. After the laser sintering step, the thickness of the layer is reduced by 175-225 nm and thus the thickness reduction ratio is about 50-55% depending upon the exposure duration and uniformity of coating thickness and uniformity of sintering across the area. The residual layer thickness can be further reduced by improving sintering quality using higher powered laser or the post-processing heat treatment. In theory, the volume percentage estimate of the Ag in the spin coated layer limits the maximum thickness reduction ratio. For the above samples, assuming a spin coated layer density of 30-35% of bulk Ag density (similar to density of spin coated layers obtained by authors in [36]), volume % estimate in the spin coated layers is estimated to be between 21 and 27% and hence, further scope of layer thickness reduction and enhancing sintering quality as indicated by the post-processing heat treatment(see supplementary material S1- volume fraction estimate for details).

Optics EXPRESS

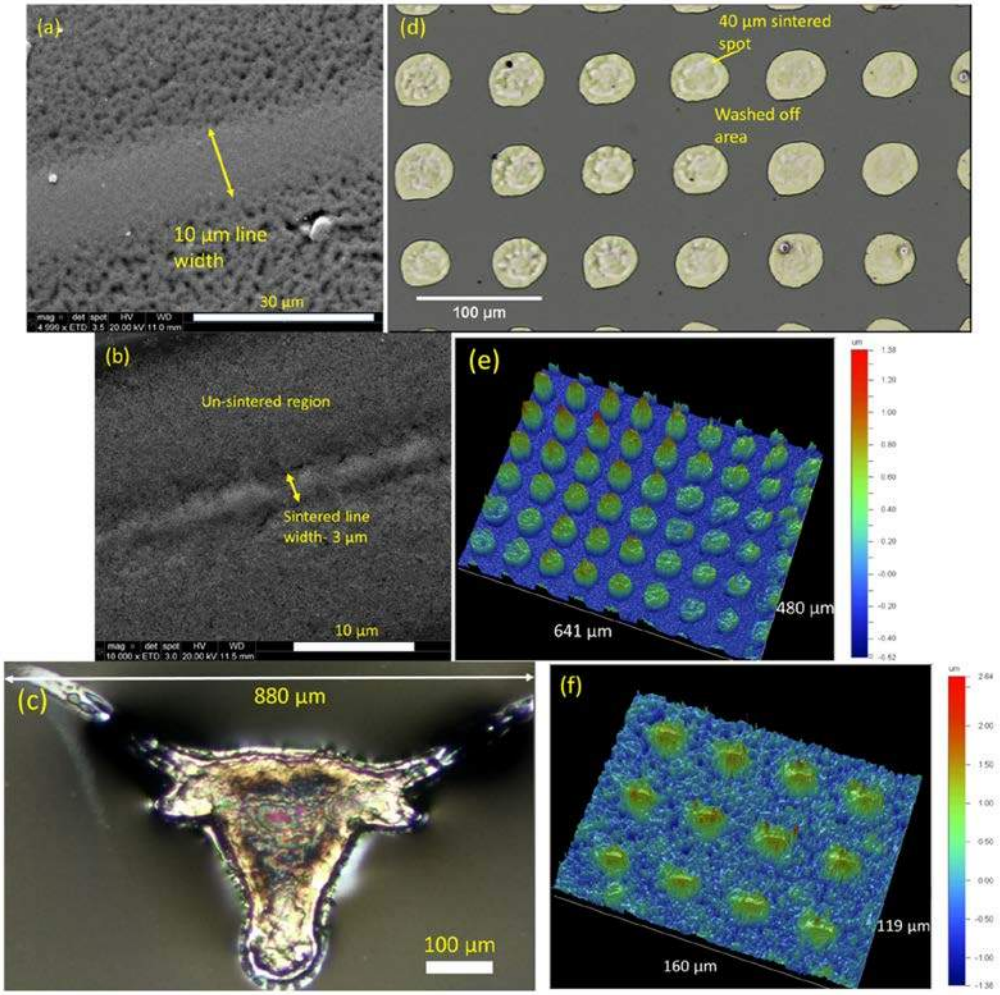

Fig. 5. A collage of different images of sintered patterns- (a) an SEM image showing a single 10 µm sintered line on an unwashed sample (b) an SEM image of a 3µm wide sintered line (c) Optical microscope image of a sintered Texas Longhorn logo (d) Optical microscope image of a washed and sintered sample with an array of 40 µm diameter spots with 80 µm pitch (e) 3D rendering of surface topography of the spots mentioned in part d (f) Surface topography of an array of 10 µm diameter sintered spots with 40 µm pitch.

6. Throughput estimate

Using a 100 ms total time estimate for sintering (including previously estimated 50 ms sintering time [36] and 50 ms for wafer stage motion- step & reaching steady state [37]) a 2.34 mm by 1.32 mm area of 1µm thick layer; the areal throughput sintering estimate is calculated to be 1112 cm^2/hr or about 44 wafers (50 mm X 50 mm) in an hour with single layer sintering. The spreader system is capable of applying a layer of nanoparticles on the 50 mm X 50 mm wafer in approximately one minute. Considering both the coating and sintering times, the maximum possible volumetric throughput with consistent 1µm thickness layers is estimated to be 63 mm^3/hr which is larger than any of the micro-AM processes available currently for metals (see supplementary material S2).

Optics EXPRESS

7. Conclusion

In this study we introduced a large area fine resolution sintering optics design to sinter a 2.3 mm by 1.3 mm area of sub-μm thick metal nanoparticle layer with an optical resolution of 1.2 μm in one shot. This design allows for the application of the system in high throughput metal/polymer micro-AM production environments such as fabrication of IC packaging building blocks, fabrication of 3D microcomponents/assemblies for applications in micro-electromechanical systems (MEMS), biochips, photonic crystals, microfluidic chips, microsensors, and micro-optoelectromechanical systems (MOEMS) along with other possible applications [38–40].

Funding

NXP Semiconductors; National Science Foundation (1728313).

Acknowledgment

The authors would like to thank Richard Piner, Texas Materials Institute, UT Austin for his assistance with profilometer measurements.

Disclosures

The authors declare that there are no conflicts of interest related to this article.

References

1. L. Alting, F. Kimura, H. N. Hansen, and G. Bissacco, “Micro engineering,” CIRP Ann. Technol. **52**(2), 635–657 (2003).
2. M. Vaezi, H. Seitz, and S. Yang, “A review on 3D micro-additive manufacturing technologies,” Int. J. Adv. Manuf. Technol. **67**(5–8), 1721–1754 (2013).
3. K. Best, R. McCleary, R. Hollman, and P. Holmes, "Advanced lithography and electroplating approach to form high-aspect ratio copper pillars," in *International Symposium on Microelectronics* (2015), (1), pp. 793–798.
4. J. U. Knickerbocker, C. S. Patel, P. S. Andry, C. K. Tsang, L. P. Buchwalter, E. J. Sprogis, H. Gan, R. R. Horton, R. J. Polastre, S. L. Wright, and others, “3-D silicon integration and silicon packaging technology using silicon through-vias,” IEEE J. Solid-State Circuits **41**(8), 1718–1725 (2006).
5. J. P. Gambino, S. A. Adderly, and J. U. Knickerbocker, “An overview of through-silicon-via technology and manufacturing challenges,” Microelectron. Eng. **135**, 73–106 (2015).
6. A. Syed, K. Dhandapani, R. Moody, L. Nicholls, and M. Kelly, "Cu Pillar and μ-bump electromigration reliability and comparison with high pb, SnPb, and SnAg bumps," in *Proceedings - Electronic Components and Technology Conference* (2011), pp. 332–339.
7. S. Lee, Y. X. Guo, and C. K. Ong, "Electromigration effect on Cu-pillar(Sn) bumps," Electron. Packag. Technol. Conf. 2005. EPTC 2005. Proc. 7th **1**, 5 pp. (2005).
8. W. W. Flack, H. A. Nguyen, E. Capsuto, and C. McEwen, "Characterization of a thick copper pillar bump process," in *Proceedings of the International Symposium and Exhibition on Advanced Packaging Materials Processes, Properties and Interfaces* (2008), pp. 208–213.
9. J. H. Lau, “Recent Advances and New Trends in Flip Chip Technology,” J. Electron. Packag. **138**(3), 30802 (2016).
10. K. M. Takahashi, “Transport Phenomena That Control Electroplated Copper Filling of Submicron Vias and Trenches,” J. Electrochem. Soc. **146**(12), 4499 (1999).
11. S. Castaldi, D. Fritz, and R. Schaeffer, “Limits of copper plating in high aspect ratio microvias,” Circuit World **25**(2), 35–40 (1999).
12. Nanoscribe, "Next Generation of 3D Laser Lithography: Photonic ProfessionalGT - Faster Than Ever!," (2015).
13. J.-U. Park, M. Hardy, S. J. Kang, K. Barton, K. Adair, D. K. Mukhopadhyay, C. Y. Lee, M. S. Strano, A. G. Alleyne, J. G. Georgiadis, P. M. Ferreira, and J. A. Rogers, "High-resolution electrohydrodynamic jet printing," Nat. Mater. **6**(10), 782–789 (2007).
14. J. A. Lewis, “Direct Ink Writing of 3D Functional Materials,” Adv. Funct. Mater. **16**(17), 2193–2204 (2006).
15. C. Spadaccini, J. Kuntz, E. Duoss, and I. Urbana-champaign, "Additive manufacturing techniques deliver three-dimensional microstructures with previously unobtainable material properties," Lawrence Livermore Natl. Lab. Sci. Technol. Rev. (March), 14–20 (2012).
16. M. M. Sundaram, A. B. Kamaraj, and V. S. Kumar, “Mask-Less Electrochemical Additive Manufacturing : A Feasibility Study,” J. Manuf. Sci. Eng. **137**, 21006 (2015).
17. Optomec, "Aerosol Jet 300 Series systems for Development of Printed Electronics and Biologics," (2015).
18. S. D. Allen, “Laser chemical vapor deposition: A technique for selective area deposition,” J. Appl. Phys. **52**(11), 6501–6505 (1981).

Optics EXPRESS

19. K. Edstro m, D. Brandell, T. Gustafsson, and L. Nyholm, "Electrodeposition as a Tool for 3D Microbattery Fabrication," Interface Mag. **20**(2), 41–46 (2011).
20. L. Besra and M. Liu, "A review on fundamentals and applications of electrophoretic deposition (EPD)," Prog. Mater. Sci. **52**(1), 1–61 (2007).
21. L. E. Ocola, C. Rue, and D. Maas, "High-resolution direct-write patterning using focused ion beams," MRS Bull. **39**(4), 336–341 (2014).
22. E. e-M. Solutions, "Systems and Equipment for Metal Manufacturing," https://www.eos.info/systems_solutions/metal.
23. L. M. Processing, "Selective laser sintering," https://www.3dsystems.com/on-demand-manufacturing/selective-laser-sintering.
24. K. An, S. Hong, S. Han, H. Lee, J. Yeo, and S. H. Ko, "Selective sintering of metal nanoparticle ink for maskless fabrication of an electrode micropattern using a spatially modulated laser beam by a digital micromirror device," ACS Appl. Mater. Interfaces **6**(4), 2786–2790 (2014).
25. Y. Son, T. W. Lim, J. Yeo, S. H. Ko, and D.-Y. Yang, "Fabrication of Nanoscale Conductors by Selective Femptosecond Laser Sintering of Metal Nanoparticles," in *Proc. 10th IEEE Int. Conf. Nanotechnol*. (2010), 390–393.
26. S. H. Ko, H. Pan, C. P. Grigoropoulos, C. K. Luscombe, J. M. J. Fráchet, and D. Poulikakos, "Air stable high resolution organic transistors by selective laser sintering of ink-jet printed metal nanoparticles," Appl. Phys. Lett. **90**(14), 2719162 (2007).
27. M. Zenou, O. Ermak, A. Saar, and Z. Kotler, "Laser sintering of copper nanoparticles," J. Appl. Phys. D **25501**, 025501 (2013).
28. Y. Son, Y. Son, J. Yeo, H. Moon, T. W. Lim, S. Hong, and K. H. Nam, "Nanoscale Electronics : Digital Fabrication by Direct Femtosecond Laser Processing of Metal Nanoparticles," Adv. Mater. **23**(28), 3176-3181 (2011).
29. Y. Son, J. Yeo, C. W. Ha, J. Lee, S. Hong, K. H. Nam, D. Y. Yang, and S. H. Ko, "Application of the specific thermal properties of Ag nanoparticles to high-resolution metal patterning," Thermochim. Acta **542**, 52–56 (2012).
30. J. Yeo, G. Kim, S. Hong, M. S. Kim, D. Kim, J. Lee, H. B. Lee, J. Kwon, Y. D. Suh, H. W. Kang, H. J. Sung, J. H. Choi, W. H. Hong, J. M. Ko, S. H. Lee, S. H. Choa, and S. H. Ko, "Flexible supercapacitor fabrication by room temperature rapid laser processing of roll-to-roll printed metal nanoparticle ink for wearable electronics application," J. Power Sources **246**, 562–568 (2014).
31. J. Yeo, S. Hong, D. Lee, N. Hotz, M. Lee, C. P. Grigoropoulos, and S. H. Ko, "Next Generation Non-Vacuum, Maskless," Low Temperature Nanoparticle Ink Laser Digital Direct Metal Patterning for a Large Area Flexible Electronics **7**(8), 1–9 (2012).
32. N. K. Roy, D. Behera, O. G. Dibua, C. S. Foong, and M. A. Cullinan, *A Novel Microscale Selective Laser Sintering (μ-SLS) Process for the Fabrication of 3D Electronic Parts*, working Paper (2018).
33. T. Instruments and I. Dlps "DLP6500FLQ 0 . 65 1080p MVSP Type A DMD," (2014).
34. H. Lee, J. Kwon, W. S. Shin, H. R. Kim, J. Shin, H. Cho, S. Han, J. Yeo, and S. Hong, "Large-area compatible laser sintering schemes with a spatially extended focused beam," Micromachines (Basel) **8**(5), 153 (2017).
35. I. Theodorakos, F. Zacharatos, R. Geremia, D. Karnakis, and I. Zergioti, "Selective laser sintering of Ag nanoparticles ink for applications in flexible electronics," Appl. Surf. Sci. **336**, 157–162 (2015).
36. N. K. Roy, O. G. Dibua, W. Jou, F. He, J. Jeong, Y. Wang, and M. A. Cullinan, "A Comprehensive Study of the Sintering of Copper Nanoparticles Using Femtosecond, Nanosecond, and Continuous Wave Lasers," J. Micro Nano-Manufacturing **6**(1), 10903 (2017).
37. N. K. Roy and M. A. Cullinan, "Fast Trajectory Tracking of a Flexure-based, Multi-Axis Nanopositioner with 50 mm Travel," IEEE/ASME Trans. Mechatron., in review.
38. K.-S. Lee, R. H. Kim, D.-Y. Yang, and S. H. Park, "Advances in 3D nano/microfabrication using two-photon initiated polymerization," Prog. Polym. Sci. **33**(6), 631–681 (2008).
39. Y. Qin, "Overview of micro-manufacturing," in *Micro-Manufacturing Engineering and Technology* (2010), pp. 1–23.
40. W. L. Jin, X. L. Phung, B. Kim, G. Lim, and D. W. Cho, "Fabrication and characteristic analysis of a poly(propylene fumarate) scaffold using micro-stereolithography technology," J. Biomed. Mater. Res. B Appl. Biomater. **87**(1), 1–9 (2008).

Supplementary materials

S1. Volume % estimate of Ag in spin coated layer

Assume that the

Density of spin coated layers is 30-35% of the density of bulk Ag (similar to the density of spin coated layers obtained by the authors in [36]

Optics EXPRESS

$$Let\ the\ mass\ of\ the\ spin\ coated\ Ag\ ink\ layer, m_{Total}\ be 1g;$$

$$Density\ of\ bulk\ silver, \rho_1 = 10.5\ g/cm^3$$

$$Density\ of\ fluid\ \left(assuming\ the\ density\ of\ fluid\ in\ the\ ink\ is\ same\ as\ the\ primary\ solvent\right), \rho_2$$

$$= 1.12\frac{g}{cm^3}\ (density\ of\ diethylene\ glycol)$$

$$Density\ of\ spin\ coated\ layer, \rho_T = 30\%\ of\ 10.5\ g/cm^3 = 3.15\ g/cm^3$$

$$Mass\ of\ Ag\ nanoparticles\ in\ the\ layer, m_1 = Let\ it\ be\ x\ g$$

$$Volume\ of\ Ag\ nanoparticles\ in\ the\ layer, V_1 = \frac{x}{10.5}cm^3$$

$$Mass\ of\ fluid\ left\ in\ the\ layer, m_2 = (1-x)\ g$$

$$Volume\ of\ fluid\ in\ the\ layer, V_2 = \frac{1-x}{1.12}cm^3$$

$$Total\ volume\ of\ the\ spin\ coated\ layer, V_{Total} = \frac{Total\ mass, m_{Total}}{\left(Density\ of\ spin\ coated\ layer\right)}$$

$$= \frac{1g}{\frac{3.15g}{cm^3}} = 0.3175cm^3 \quad (7)$$

$$Also, Total\ volume\ of\ the\ spin\ coated\ layer, V_{Total}$$

$$= Volume\ of\ Ag\ nanoparticle + Volume\ of\ the\ fluid = V_1 + V_2 \quad (8)$$

$$= \left(\frac{x}{10.5} + \frac{1-x}{1.12}\right)cm^3$$

$$Equating\ (7)\ and\ (8)$$

$$x = 0.7213$$

$$Volume\ fraction\ of\ Ag = \frac{V_1}{V_{Total}} = \frac{\frac{x}{10.5}}{0.3175}$$

$$= 0.2163\left(assuming\ spin\ coated\ layer\ density\ to\ be\ 30\%\ of\ the\ density\ of\ bulk\ Ag\ density\right)$$

$$= 0.2723\ (assuming\ spin\ coated\ layer\ density\ to\ be\ 35\%\ of\ the\ density\ of\ bulk\ Ag\ density\ )$$

S2. Throughput estimation

Considering a coating and wafer prep. time of approximately 1 minute per layer, the throughput of the process is estimated to be 63 mm^3/hr according to the calculations shown below:

Time to sinter one complete 50 X 50 mm wafer under the optical system assuming a previously obtained sintering time of 100 ms =

$$= \frac{50\ X\ 50}{2.3\ X\ 1.3} = 821*100\ ms = 82.1s$$

Time to fully coat and prepare the sample for sintering = 60s

Limiting process in the current system per layer is optical system.

Total time for sintering 1 layer with 1 μm thickness= 82+60= 142 s

Max. volume sintered (assuming full coverage) = 50mm X 50 mm X 0.001 mm= 2.5 mm^3

Max. volumetric throughput for the process= 2.5 mm^3/142s= 2.5*3600/142 mm^3/hr= 63 mm^3/ hr.